Geranylgeranyl-Regulated Transport of the Prenyltransferase UBIAD1 between Membranes of the ER and Golgi

Marc M. Schumacher[‡], Dong-Jae Jun[‡], Youngah Jo, Joachim Seemann[¶], and Russell A. DeBose-Boyd[§]

From the Departments of Molecular Genetics and Cell Biology[¶], University of Texas Southwestern Medical Center, Dallas, TX 75390-9046

[‡]These authors contributed equally to this work.

[§]To whom correspondence may be addressed. Dr. Russell DeBose-Boyd, 5323 Harry Hines Blvd., Dallas, TX 75390-9046. E-mail: Russell.DeBose-Boyd@utsouthwestern.edu.

Running Title: *Regulated transport of UBIAD1 between ER and Golgi*

Abbreviations:

ER, endoplasmic reticulum; FCS, fetal calf serum; GGpp, geranylgeranyl pyrophosphate; GGOH, geranylgeraniol; HMG CoA, 3-hydroxy-3-methylglutaryl coenzyme A; LPDS, lipoprotein-deficient serum; MD, menadione; MK-4, menaquinone-4; PK, phylloquinone; SCD, Schnyder corneal dystrophy; UBIAD1, UbiA prenyltransferase domain-containing protein-1.

Abstract

UbiA prenyltransferase domain-containing protein-1 (UBIAD1) utilizes geranylgeranyl pyrophosphate (GGpp) to synthesize the vitamin K_2 subtype menaquinone-4. Previously, we found that sterols trigger binding of UBIAD1 to endoplasmic reticulum (ER)-localized HMG CoA reductase, the rate-limiting enzyme in synthesis of cholesterol and nonsterol isoprenoids including GGpp. This binding inhibits sterol-accelerated degradation of reductase, which contributes to feedback regulation of the enzyme. The addition to cells of geranylgeraniol (GGOH), which can become converted to GGpp, triggers release of UBIAD1 from reductase, allowing for its maximal degradation and permitting ER-to-Golgi transport of UBIAD1. Here, we further characterize geranylgeranyl-regulated transport of UBIAD1. Results of this characterization support a model in which UBIAD1 continuously cycles between the ER and medial/trans Golgi of isoprenoid-replete cells. Upon sensing a decline of GGpp in ER membranes, UBIAD1 becomes trapped in the organelle where it inhibits reductase degradation. Mutant forms of UBIAD1 associated with Schnyder corneal dystrophy (SCD), a human eye disease characterized by corneal accumulation of cholesterol, are sequestered in the ER and block reductase degradation. Collectively, these findings disclose a novel sensing mechanism that allows for stringent metabolic control of intracellular trafficking of UBIAD1, which directly modulates reductase degradation and becomes disrupted in SCD.

Keywords: endoplasmic reticulum, Golgi, lipid metabolism, isoprenoid, protein trafficking, vitamin K

Introduction

UbiA prenyltransferase domain-containing protein-1 (UBIAD1) belongs to the UbiA superfamily of integral membrane prenyltransferases (1). These enzymes contain 8-10 transmembrane helices and catalyze transfer of isoprenyl groups to aromatic acceptors, producing a wide range of molecules such as ubiquinones, hemes, chlorophylls, vitamin E, and vitamin K. In animals, UBIAD1 catalyzes transfer of the 20-carbon geranylgeranyl moiety from geranylgeranyl pyrophosphate (GGpp) to menadione released from plant-derived phylloquinone, thereby generating the vitamin K_2 subtype menaquinone-4 (MK-4) (2, 3).

Mutations in the UBIAD1 gene are associated with Schnyder corneal dystrophy (SCD), an autosomal dominant human eye disease characterized by progressive opacification of the cornea, owing to abnormal accumulation of cholesterol and other lipids (4, 5). Systemic dyslipidemia appears to be associated with some, but not all SCD cases (6, 7). Missense mutations that alter 20 amino acid residues in UBIAD1 have been identified in ~50 SCD families (8, 9). Several of these altered amino acids reside within the active site of UBIAD1 (10, 11). A link between UBIAD1 and cholesterol metabolism was first provided by co-immunoprecipitation studies that showed an association of UBIAD1 with the cholesterol biosynthetic enzyme 3-hydroxy-3-methylglutaryl coenzyme A (HMG CoA) reductase (8). More recently, we showed that UBIAD1 inhibits sterol-accelerated, endoplasmic reticulum-associated degradation (ERAD) of reductase (12), one of several feedback mechanisms that converge on the enzyme to maintain cholesterol homeostasis (13).

The polytopic, ER-localized HMG CoA reductase catalyzes reduction of HMG CoA to mevalonate, a rate-limiting step in synthesis of cholesterol as well as nonsterol isoprenoids including farnesyl pyrophosphate (Fpp) and GGpp that are transferred to many cellular proteins and utilized in synthesis of ubiquinone, MK-4, heme, and dolichol (2, 13, 14). Intracellular accumulation of sterols causes reductase to bind ER membrane proteins called Insigs (15, 16), which leads to ubiquitination of the enzyme by Insig-associated ubiquitin ligases (16-19). Ubiquitinated reductase is then extracted across ER membranes and released into the cytosol for degradation by 26S proteasomes (20, 21). Maximal degradation requires the addition to cells of geranylgeraniol (GGOH), the alcohol derivative of GGpp (16). We postulate that GGOH becomes converted to GGpp, which augments reductase ERAD by enhancing its membrane extraction (21). Recently, we found that sterols also cause reductase to bind to UBIAD1 (12). GGpp triggers release of UBIAD1 from reductase, allowing for its maximal ERAD. Importantly, the addition to cells of farnesol, the alcohol derivative of Fpp,

neither inhibits the binding of UBIAD1 to reductase nor augments ERAD of reductase (12, 16). Two of the twenty SCD-associated mutants of UBIAD1 (N102S and G177R) resist GGpp-induced displacement from reductase and thereby blocked its degradation (12).

In the course of our studies, we discovered that GGpp also stimulates translocation of UBIAD1 from the ER to the Golgi (12). SCD-associated UBIAD1 (N102S) and (G177R) are refractory to this GGpp-induced Golgi transport and localize to the ER. Building on these observations, we show in the current study that UBIAD1 localizes to the medial-trans cisternae of the Golgi in isoprenoid-replete cells. All 20 of the SCD-associated mutants of UBIAD1 are defective in Golgi transport and remain sequestered in the ER where they inhibit reductase ERAD in a seemingly dominant-negative fashion. Intriguingly, acute depletion of isoprenoids triggers rapid retrograde transport of UBIAD1 from the Golgi to the ER. Although UBIAD1 localizes to the Golgi of isoprenoid-replete cells in the steady state, the protein accumulates in the ER when transport from the organelle is blocked. These findings suggest a model in which UBIAD1 constitutively cycles between the Golgi and ER. Upon sensing GGpp depletion in membranes of the ER, UBIAD1 becomes trapped in the organelle and inhibits reductase ERAD so as to stimulate mevalonate synthesis for replenishment of GGpp. This novel sensing mechanism directly controls ERAD of reductase and becomes disrupted in SCD, which likely contributes to the accumulation of cholesterol that characterizes the eye disease.

Materials and Methods

Materials – We obtained geranylgeraniol, geranylgeranyl pyrophosphate, farnesyl pyrophosphate, and brefeldin-A from Sigma-Aldrich (St. Louis, MO) and Santa Cruz Biotechnology (Dallas, TX); cycloheximide was obtained from Cell Signaling Technology (Danvers, MA); 25-hydroxycholesterol and cholesterol was obtained from Steraloids (Newport, RI); hydroxypropyl β-cyclodextrin was obtained from (Cyclodextrin Technologies Development, Alachua, FL). Recombinant His-tagged $Sar1^{DN}$ was expressed in *E. coli* and isolated on Ni-NTA agarose (Qiagen, Valencia, CA) as previously described (22). The buffer was exchanged by dialysis against 25 mM Hepes-KOH, pH 7.2, 125 mM potassium acetate, 1 mM $MgCl_2$, 1 mM glutathione, 10 μM guanosine diphosphate, and 50 μM EGTA. SR-12813 was synthesized by the Core Medicinal Chemistry laboratory at the University of Texas Southwestern Medical Center or obtained from

Sigma-Aldrich. Other reagents, including new born calf lipoprotein-deficient serum (LPDS, d > 1.215 g/ml), sodium compactin, and sodium mevalonate, were prepared or obtained as previously described (20, 23).

Expression Plasmids – The expression plasmids pCMV-Myc-UBIAD1, which encodes human UBIAD1 containing a single copy of a Myc epitope at the N-terminus under transcriptional control of the cytomegalovirus (CMV) promoter, pCMV-Myc-UBIAD1 (N102S) encoding Myc-tagged human UBIAD1 harboring the SCD-associated asparagine-102 to serine (N102S) mutation, and pCMV-Myc-UBIAD1 (G177R) encoding Myc-tagged human UIBAD1 harboring the SCD-associated glycine-177 to arginine mutation, were previously described (12). The remaining SCD-associated mutants of UBIAD1 were generated using the QuikChange® Site-Directed Mutagenesis Kit (Agilent Technologies, Santa Clara, CA) and pCMV-Myc-UBIAD1 as a template. The cDNA encoding human calnexin was purchased from Open Biosystems (Lafayette, CO) and subcloned into pcDNA3.1(+) using standard PCR methods. The expression plasmid pCMV-mCherry-calnexin was generated by fusing mCherry derived from the pmCherry-C1 vector (Clontech, Mountain View, CA) to the N-terminus of calnexin. The expression plasmid pDsRed-Golgi encoding a fusion protein consisting of DsRed-Monomer and the N-terminal 81 amino acids of human β1,4-galactosyltransferase was obtained from Clontech.

Cell Culture – SV-589 cells are a line of immortalized human fibroblasts expressing the SV40 large T-antigen (24). Monolayers of SV-589 cells were maintained in medium A (DMEM containing 1000 mg glucose/l, 100 U/ml penicillin, and 100 µg/ml streptomycin sulfate) supplemented with 10% (vol/vol) fetal calf serum (FCS) at 37 ºC, 5% CO_2. SV-589/pMyc-UBIAD1 cells, a line of SV-589 cells that stably express Myc-UBIAD1, were generated by transfection of SV-589 cells with 3 µg pCMV-Myc-UBIAD1 using FuGENE6 transfection reagent (Promega, Madison, WI) as described below, followed by 2 weeks of selection in medium A supplemented with 10% FCS and 700 µg/ml G418. Individual colonies were isolated using cloning cylinders. Clonal isolates from expanded colonies were obtained using serial dilution in 96-well plates. Clones were evaluated by immunofluorescence microscopy using IgG-9E10 against the Myc epitope (described below).

CHO-K1/pMyc-UBIAD1 and UT-2/pMyc-UBIAD1, lines of CHO-K1 and reductase-deficient UT-2 cells (25) that stably express Myc-UBIAD1, were generated by transfection of cells with 3 µg pCMV-Myc-UBIAD1 as described below, followed by 2 weeks of selection in medium B (1:1 mixture of Ham's F-12 medium and DMEM containing 100

U/ml penicillin and 100 µg/ml streptomycin sulfate) containing with 5% FCS and 700 µg/ml G418. The medium for UT-2 cells was further supplemented with 200 µM mevalonate. Individual colonies were isolated using cloning cylinders, and expression of Myc-UBIAD1 was determined by immunoblot analysis. Select colonies were expanded and then further purified by serial dilution in 96-well plates. Individual clones were screened by immunofluorescence using IgG-9E10 as described below. CHO-K1/pMyc-UBIAD1 cells were maintained in monolayer in medium B containing 5% FCS and 700 µg/ml G418 at 37 ºC, 8% CO_2. Monolayers of UT-2/pMyc-UBIAD1 cells were grown at 37 ºC, 8% CO_2 in identical medium supplemented with 200 µM mevalonate.

CHO-7 cells, a subline of CHO-K1 cells selected for growth in LPDS (26), were grown in monolayer at 37 ºC, 8% CO_2. The cells were maintained in medium B supplemented with 5% LPDS. Monolayers of SRD-13A/pGFP-Scap, a line of Scap-deficient CHO-7 cells that stably express GFP-Scap (27), were maintained at 37 ºC, 8% CO_2 in medium B supplemented with 5% LPDS.

Transfection and immunofluorescence – Transient transfection of SV-589 and CHO-7 cells with FuGENE6 transfection reagent was carried out as previously described (12, 15). Conditions of subsequent incubations are described in the figure legends. Following incubations, cells were washed with PBS and subsequently fixed and permeabilized for 15 min in methanol at -20°C. Upon blocking with 1 mg/ml BSA in PBS, coverslips were incubated for 1 h at 37°C with primary antibodies (IgG-H8, a mouse monoclonal antibody against human UBIAD1 (Santa Cruz Biotechnology, Dallas, TX), rabbit polyclonal anti-GM130 IgG (28), IgG-9E10, a mouse monoclonal antibody against c-Myc purified from the culture medium of hybridoma clone 9E10 (American Type Culture Collection, Manassas, VA), and rabbit polyclonal anti-TGN46 (Abcam, Cambridge, MA)) diluted in PBS containing 1 mg/ml BSA. Bound antibodies were visualized with goat anti-mouse IgG conjugated to Alexa Fluor 488 or Alexa Fluor 594 and goat anti-rabbit Alexa Fluor 594 (Life Technologies, Grand Island, NY) as described in the figure legends. Coverslips were also stained for 5 min with 300 nM 4',6-diamidino-2-phenylindole (DAPI) (Life Technologies, Grand Island, NY) to visualize nuclei. The coverslips were then mounted in Mowiol 4-88 solution (Calbiochem/EMD Millipore, Billerica, MA) or Fluoromount G (Electron Microscopy Sciences, Hatfield, PA). Fluorescence imaging was performed using a DeltaVision Microscopy Imaging System (GE Healthcare Life Sciences, Pittsburgh, PA) equipped with a CoolSNAP HQ^2 camera (Photometrics, Tucson, AZ) and objective oil lenses 60x/1.42 and 100x/1.40 (Olympus, Waltham, MA) as indicated in figure legends. Z stacks were deconvolved and

Pearson correlation coefficients for each z stack were generated using DeltaVision SoftWoRx software (GE Healthcare Life Sciences, Pittsburgh, PA). Additional fluorescence imaging was performed using a Zeiss Axio Observer Epifluorescence microscope using a 63x/1.4 oil Plan-Apochromat objective and Zeiss Axiocam color digital camera (Zeiss, Peabody, MA) in black&white mode as indicated in figure legends. Brightness levels were adjusted across the entire images using ImageJ software (National Institution of Health, USA).

Preparation of cytosol – Rat liver cytosol was prepared from adult male Sprague-Dawley rats as previously described (29). Cytosol from isoprenoid-depleted UT-2 cells was prepared as follows. UT-2 cells were set up on day 0 at 3 X 10^5 cells per 100-mm dish in medium B containing 5% FCS and 200 µM mevalonate. On day 3, cells were depleted of isoprenoids though incubation in medium B supplemented with 5% FCS in the absence of mevalonate. After 16 h at 37 ºC, cells were harvested into the medium by scraping and collected by centrifugation, after which cell pellets were washed with PBS supplemented with a protease inhibitor cocktail consisting of 20 µM leupeptin, 5 µg/ml pepstatin A, 2 µg/ml aprotinin, 25 µg/ml N-acetyl-leucinal-leucinal-norleucinal, and 1 mM dithiotheitol. The washed cells from 250 dishes were resuspended in buffer containing 50 mM HEPES-KOH, pH 7.2, 250 mM sorbitol, 70 mM potassium acetate, 5 mM potassium EGTA, and 2.5 mM magnesium acetate supplemented with protease inhibitors. The resuspended cells were then lysed by passage though an 18-gauge needle 30 times, followed by 25 strokes in a 50 ml Dounce homogenizer fitted with a teflon pestle. The resulting homogenates were subjected to centrifugation at 1000 X g for 10 min at 4 ºC. The supernatant of this spin was then subjected to centrifugation at 100,000 X g for 1 h at 4 ºC. The final supernatant, designated as cytosol (~ 2 mg/ml), was divided into multiple aliquots, snap frozen in liquid nitrogen, and stored at -80 ºC. For experiments, tubes were thawed in a 37 ºC water bath and placed on ice until use.

In vitro vesicle-formation assay – SV-589 cells were set up for experiments as described in the figure legends. Following incubations described in figure legends, cells were harvested into medium by scraping and pooled suspensions from triplicate dishes were subjected to centrifugation at 1000 X g for 5 min at 4 ºC. Cell pellets were resuspended in 0.5 ml buffer containing 10 mM HEPES-KOH, pH 7.2, 250 mM sorbitol, 10 mM potassium acetate, 1.5 mM magnesium acetate and protease inhibitors, passed through a 22-gauge needle 30 times, and centrifuged at 1000 X g for 5 min at 4 ºC. The resulting supernatants were transferred to siliconized microfuge tubes and centrifuged at 16,000 X g for 3 min at 4 ºC.

Each pellet was suspended in 50 µl of buffer containing 50 mM HEPES-KOH, pH 7.2, 250 mM sorbitol, 70 mM potassium acetate, 5 mM potassium EGTA, 2.5 mM magnesium acetate, and protease inhibitors to obtain microsomes that were pooled and used in the *in vitro* vesicle-formation assay described below. The protein concentration of an aliquot (5 µl) of microsomal suspensions were determined using Pierce™ Coomassie Plus Protein Assay Reagent (ThermoFisher Scientific, Waltham, MA) according to the manufacturer's instructions using BSA as standard.

The protocol used in this study was adapted from previously described procedures (27, 30, 31). In a final volume of 100 µl, each reaction contained 50 mM HEPES-KOH, pH 7.2, 250 mM sorbitol, 70 mM potassium acetate, 5 mM potassium EGTA, 2.5 mM magnesium acetate, 1.5 mM ATP, 0.5 mM GTP, 10 mM creatine phosphate, 4 units/ml of creatine kinase, protease inhibitors, 80-100 µg protein of SV-589 microsomes, and 10-100 µg rat liver or UT-2 cytosol. Incubations were carried out in siliconized 1.5 ml microfuge tubes for 20 min at 37 ºC (unless otherwise indicated). Reactions were terminated by transfer of tubes to ice, followed by centrifugation at 16,000 X g for 3 min at 4 ºC to obtain a medium-speed pellet (P16) and a medium-speed supernatant (S16). The S16 fraction was then subjected to an additional round of centrifugation at 100,000 X g for 30 min at 4 ºC to obtain a high-speed pellet (P100). The P16 and P100 were resuspended in buffer containing 10 mM Tris-HCl, pH 7.6, 100 mM NaCl, and 1% (w/v) SDS plus protease inhibitors supplemented with 4X SDS-PAGE loading buffer and heated at 95 ºC for 5 min. Aliquots of the P16 (7.5 µl) and P100 (30 µl) were subjected to 10% SDS-PAGE, transferred to nylon filters, and analyzed by immunoblotting. The P16 and P100 fractions are referred to membranes and vesicles, respectively. Primary antibodies used for immunoblot analysis include: IgG-H8 against human UBIAD1; IgG-4H4, a mouse monoclonal antibody against hamster Scap (32); and rabbit polyclonal anti-ribophorin I IgG (Abcam, Cambridge, MA).

Microinjection of SV-589/pMyc-UBIAD1 cells – Microinjection was performed with a Transjector 5246 and a Micromanipulator 5171 (Eppendorf, Hauppauge, NY). SV-589/pMyc-UBIAD1 cells on glass coverslips were changed to medium A containing 50 mM Hepes/KOH, pH7.4 and 10% FCS and injected into the cytoplasm with 1 mg/ml $Sar1^{DN}$ or 1 mg/ml BSA as a control together with 2 mg/ml lysine fixable 70 kDa Texas-Red conjugated Dextran (Invitrogen, Waltham, MA) as injection marker. Following incubation for 3 h at 37 ºC, the cells were fixed with 3.7% formaldehyde in PBS for 15 min at room temperature and permeabilized for 10 min in methanol at -20°C. Upon blocking with 1 mg/ml BSA in PBS, the cells were labeled with the indicated monoclonal primary antibodies (IgG-9E10 against Myc or anti-

GM130 (BD Biosciences, San Jose, CA) followed by Alexa Fluor 488 -conjugated goat anti-mouse secondary antibodies. DNA was stained for 5 min with 1 μg/ml Hoechst 33342 (Invitrogen) in PBS. Epifluorescence images were obtained using a Plan-Neofluar 40x/1.3 DIC objective (Zeiss, Oberkochen, Germany), an Axiovert 200M microscope (Zeiss), an Orca 285 camera (Hamamatsu, Hamamatsu City, Japan), and the software Openlab 4.0.2.

Results

Fig. 1A shows that endogenous UBIAD1 localized to ER membranes when SV-589 cells, a line of transformed human fibroblasts (24), were depleted of sterol and nonsterol isoprenoids through incubation for 16 h in medium containing lipoprotein-deficient serum (LPDS) and the reductase inhibitor compactin (panel 1). The addition of GGOH to the cells stimulated translocation of UBIAD1 from the ER to the Golgi in a time-dependent manner (panels 2-6). GGOH-induced transport of UBIAD1 to the Golgi continued in the presence of the protein synthesis inhibitor cycloheximide (**Fig. 1B**). The nonsterol isoprenoid similarly stimulated ER-to-Golgi transport of Myc-UBIAD1 in SV-589/pMyc-UBIAD1 cells, which stably overexpress the protein (**Fig. 1C**). **Fig. 1D** compares the subcellular localization of Myc-UBIAD1 with that of Scap, a membrane protein whose transport from the ER to the Golgi is regulated by sterols (27, 33). The results show that a majority of Myc-UBIAD1 localized to the Golgi of sterol-replete SRD-13A/pGFP-Scap cells (**Fig. 1D**, panel 1), Scap-deficient Chinese hamster ovary (CHO) cells that stably overexpress GFP-Scap (27). In contrast, a significant fraction of GFP-Scap was present in the ER of sterol-replete SRD-13A/pGFP-Scap cells (panel 2). When cells were depleted of isoprenoids, Myc-UBIAD1 was sequestered in the ER (panel 3), whereas GFP-Scap translocated to the Golgi (panel 4).

Deconvolution microscopy was next employed to analyze the subcellular localization of Myc-UBIAD1 in SV-589/pMyc-UBIAD1 cells. The results show that as expected, Myc-UBIAD1 co-localized with mCherry-calnexin in ER membranes of SV-589/pMyc-UBIAD1 cells deprived of isoprenoids (**Supplemental Fig. 1A**). When cells were cultured in sterol-replete FCS-containing medium, Myc-UBIAD1 co-localized with DsRed-Golgi (**Supplemental Fig. 1B**), which consists of DsRed-Monomer fused to amino acids 1-81 of β1,4 galactosyltransferase that targets the fusion protein to the medial-trans cisternae of the Golgi (34). We further analyzed the co-localization of Myc-UBIAD1 with GM130 and

TGN-46, which reside in the cis-Golgi and the trans Golgi network (TGN), respectively (35, 36). In FCS-cultured cells, we observed an apparent overlap in localization of Myc-UBIAD1 with that of GM130 (**Fig. 2**, panels 1-3), DsRed-Golgi (panels 4-6), and TGN-46 (panels 7-9). The localization of UBIAD1 within the Golgi was further substantiated by conducting an experiment in cells subjected to treatment with the microtubule depolymerization agent nocodazole. Treatment of cells with nocodazole is known to cause the Golgi ribbon to become fragmented into stacks that are dispersed throughout the cytoplasm (37). However, Golgi polarity is maintained in the presence of nocodazole, allowing visualization of individual stacks (38). When SV-589/Myc-UBIAD1 cells were treated with nocodazole, GM130, DsRed-Golgi, TGN-46, and Myc-UBIAD1 localized to scattered Golgi stacks in the cytoplasm (**Fig. 2**, panels 10-18). Co-localization of Myc-UBIAD1 with GM130 (panels 10-12) and TGN-46 (panels 16-18) was reduced in presence of nocodazole; however, co-localization of the prenyltransferase with DsRed-Golgi remained unchanged compared to untreated controls (panels 13-15, see graph below images).

Anterograde transport of proteins from the ER to the Golgi occurs through their incorporation into transport vesicles that bud from ER membranes (39, 40). Methods that reconstitute *in vitro* formation of ER-derived transport vesicles have been established (30, 31). In these studies, membranes were incubated with nucleotide triphosphates (ATP/GTP) plus an ATP regenerating system and cytosol, which led to formation of vesicles that remained in the supernatant following centrifugation at 16,000 X g, while donor membranes were pelleted. Using these methods, we next examined the *in vitro* budding of endogenous UBIAD1. In the experiment of **Fig. 3A**, cells were depleted of isoprenoids to sequester UBIAD1 in the ER. Membranes isolated from these isoprenoid-depleted cells were then incubated in absence or presence of rat liver cytosol and ATP/GTP plus the ATP-regenerating system. Following incubation at various temperatures, donor membranes and vesicles were isolated by differential centrifugation and analyzed by immunoblot. UBIAD1 appeared in vesicles when reactions were carried out at 28, 32, or 37 ºC and supplemented with ATP/GTP and cytosol (**Fig. 3A**, panel 1, lanes 5, 9, and 13). ER-resident ribophorin I remained in donor membranes and was not visualized in vesicles (panel 3), indicating their generation did not result from nonspecific membrane fragmentation. The appearance of UBIAD1 was time-dependent (**Fig. 3B**, panel 1, lanes 4, 6, and 8); Scap also appeared in vesicles generated from complete reactions (panel 3, lanes 4, 6, and 8). Moreover, budding of UBIAD1 was proportional to the amount of cytosol used in the *in vitro* budding reaction (**Fig. 3C**).

Cytosol used in **Fig. 3A-C** was obtained from livers of rats that were not depleted of isoprenoids. Thus, we reasoned that residual GGpp in the cytosol stimulated incorporation of UBIAD1 into vesicles. **Fig. 3D** reveals that addition of GGpp to cytosol obtained from isoprenoid-depleted, reductase-deficient CHO-K1 cells (designated UT-2 (25)) enhanced incorporation of UBIAD1 into vesicles (panel 1, compare lanes a-e and f-j). Importantly, this enhancement was not observed in the presence of Fpp (**Fig. 3E**, panel 1, compare lanes c-e and f-h).

Twenty-four mutations that alter twenty amino acid residues in UBIAD1 protein have been identified in SCD families (8, 9). Asparagine-102 (N102) and glycine-177 (G177) are the most frequently altered UBIAD1 residues in SCD. We previously found that these SCD-associated mutants remain sequestered in the ER of isoprenoid-replete cells (12). **Fig. 4** shows an experiment that compares the subcellular localization of wild type UBIAD1 to that of all SCD-associated mutants of the prenyltransferase. The results reveal that as expected, wild type Myc-UBIAD1 localized to the Golgi of SV-589 cells cultured in FCS (**Fig. 4**, panel 1). UBIAD1 (S75F), which is not associated with SCD and results from a moderately common polymorphism in the UBIAD1 gene (4, 5), also localized to the Golgi (panel 2). Consistent with our previous findings, UBIAD1 (N102S) and (G177R) were sequestered within membranes of the ER (panels 5 and 14, respectively). The remaining SCD-associated mutants of UBIAD1 were similarly defective in transport to the Golgi and localized to the ER (panels 3, 4, 6-13, and 15-22). However, it should be noted that four SCD-associated UBIAD1 mutants, D112G (panel 6), D118G (panel 7), R119G (panel 8), and N232S (panel 18), exhibited partial Golgi localization.

In addition to their sequestration in ER membranes of isoprenoid-replete cells, UBIAD1 (N102S) and (G177R) inhibit sterol-accelerated ERAD of reductase (12). To determine whether the other 18 SCD-associated mutants of UBIAD1 inhibit reductase ERAD, we employed SR-12813. The 1,1-bisphosphonate ester mimics sterols in accelerating reductase ERAD and prevents growth of cells in LPDS-containing medium (41), which renders them dependent on endogenous cholesterol synthesis for survival (26). Importantly, growth of CHO-7 cells (a subline of CHO-K1 cells) in the presence of SR-12813 is restored by overexpression of degradation-resistant, but not wild type reductase (41). **Fig. 5** shows that growth of mock-transfected CHO-7 cells tolerated as much as 5 μM SR-12813; proliferation was markedly reduced when cells were challenged with higher concentrations of SR-12813. Cells expressing wild type UBIAD1 were slightly more resistant to SR-12813 and tolerated up to 7.5 μM of the drug. Overexpression of any of the SCD-associated UBIAD1 mutants markedly enhanced resistance of CHO-7 cells to growth in SR-12813. Similar results were observed in at least two independent repeat experiments, one of which is shown in **Supplemental Fig. 2A**. Moreover, expression of SCD-

associated, but not wild type UBIAD1 led to elevated levels of reductase, indicating slowed ERAD of the protein (**Supplemental Fig. 2B**).

We next examined the effect of isoprenoid depletion on retrograde transport of endogenous UBIAD1 from the Golgi to the ER over time. SV-589 cells were first cultured in the presence of FCS for 16 h to ensure localization of UBIAD1 to Golgi and subsequently treated for various periods of time with compactin. The results show that Golgi localization of endogenous UBIAD1 was inhibited after 2 h of nonsterol isoprenoid depletion with compactin (**Fig. 6A**, compare panels 1 and 4). Similar results were obtained in the presence of cycloheximide (**Fig. 6B**, compare panels 1 and 2 with 3 and 4), indicating that Golgi-localized, but not newly synthesized UBIAD1 relocalized to ER upon depletion of nonsterol isoprenoids. Importantly, cycloheximide did not disrupt Golgi localization of UBIAD1 in the absence of compactin (data not shown), indicating inhibition of protein synthesis does not alter production of GGpp that promotes ER-to-Golgi transport of UBIAD1. Compactin also stimulated transport of Myc-UBIAD1 from the Golgi to the ER of SV-589/pMyc-UBIAD1 cells (**Fig. 6C**); retrograde transport occurred when cells were cultured in either sterol-replete FCS-containing medium (panels 1 and 2) or sterol-depleted medium containing LPDS (panels 3 and 4). This result is consistent with our previous observation that sterols do not influence subcellular localization of UBIAD1 (12).

Although sterols trigger its binding to UBIAD1 in ER membranes (12), reductase does not appear to directly contribute to geranylgeranyl-regulated transport of UBIAD1 between the ER and the Golgi. CHO-K1/pMyc-UBIAD1 cells are a line of CHO-K1 cells that stably overexpress Myc-UBIAD1. When these cells were cultured in the presence of FCS, Myc-UBIAD1 localized to the Golgi (**Fig. 7**, panel 1). Treatment of CHO-K1/pMyc-UBIAD1 cells with compactin disrupted Golgi localization of Myc-UBIAD1, causing its retrograde transport to the ER (panel 2); Myc-UBIAD1 remained in the Golgi when compactin-treated cells also received GGOH (panel 3). Myc-UBIAD1 localized to the ER of FCS-cultured UT-2/pMyc-UBIAD1 cells (**Fig. 7**, panel 4), which stably overexpress the protein. This result is consistent with the mevalonate auxotrophy of reductase-deficient UT-2 cells (25). Although compactin had no effect on localization of Myc-UBIAD1 in UT-2/pMyc-UBIAD1 cells (panel 5), the addition of GGOH stimulated its transport from the ER to the Golgi (panel 6).

Many Golgi-resident proteins are known to continuously recycle from the Golgi to the ER (42-44). This retrograde transport can be revealed through inhibition of export from the ER, which causes Golgi-resident proteins to accumulate in the ER (43, 44). To determine whether UBIAD1 constitutively cycles between the Golgi and the ER, we

began by employing the fungal metabolite brefeldin A (BFA). BFA inhibits GTP-exchange factors that activate the small GTPase Arf1, which initiates recruitment of coat protein complex I to Golgi membranes for retrograde transport to ER (45). This inhibition causes redistribution of Golgi proteins and membranes to the ER and indirectly blocks export from the organelle (46). **Fig. 8A** shows that BFA caused redistribution of both endogenous UBIAD1 (panels 1-4) and Myc-UBIAD1 (panels 5-8) to the ER of FCS-cultured cells. The specificity of BFA is demonstrated by the observation that UBIAD1, but not TGN-localized TGN-46, accumulated in the ER following BFA treatment (**Fig. 8B**, compare panels 1, 3, and 5 with 2, 4, and 6).

Formation of COPII vesicles, which mediate ER-to-Golgi transport of proteins, is initiated by recruitment of the GTPase Sar1 to ER membranes (47). Membrane-associated Sar1 subsequently recruits the COPII dimers Sec23/24 and Sec13/31, resulting in budding of vesicles from ER membranes that are destined for the Golgi. To directly inhibit ER export, we microinjected FCS-cultured SV-589/pMyc-UBIAD1 cells with GTP-restricted, dominant-negative Sar1 (H79G) (designated $Sar1^{DN}$). Results of **Fig. 9A** show that Myc-UBIAD1 localized to Golgi membranes of SV-589/pMyc-UBIAD1 cells microinjected with BSA (panels 1 and 2). However, Myc-UBIAD1 accumulated in the ER of SV-589/pMyc-UBIAD1 cells when they were microinjected with $Sar1^{DN}$ (panels 3 and 4). Consistent with previous studies (48, 49), GM130 remained in the Golgi of cells microinjected with $Sar1^{DN}$ (**Fig. 9A**, panels 5 and 6).

Discussion

The current results provide experimental basis for the model shown in **Fig. 9B**, which depicts the intracellular trafficking of UBIAD1. Consistent with our previous studies (12), depleting cells of isoprenoids caused UBIAD1 to become sequestered in membranes of the ER (**Fig. 1** and **Supplemental Fig. 1A**). ER-to-Golgi transport of both endogenous and overexpressed UBIAD1 was stimulated, in a time-dependent fashion, by the addition of GGOH to cells. Notably, expression of Myc-UBIAD1 in SV-589/pMyc-UBIAD1 cells exceeds that of endogenous UBIAD1 by about 30-fold (data not shown). However, the majority of Myc-UBIAD1 remained in the ER of isoprenoid-depleted cells and kinetics of its GGOH-induced ER-to-Golgi transport were similar compared to those of endogenous UBIAD1 (**Fig. 1C**). Thus, sequestration of UBIAD1 in ER of isoprenoid-depleted cells likely results from its inability to become incorporated into

transport vesicles destined for the Golgi rather than from increased association with an ER retention protein, which we anticipate would become saturated upon UBIAD1 overexpression.

When added to cells, we postulate that GGOH becomes converted to GGpp, which in turn, binds to UBIAD1 and triggers its translocation to the medial/trans Golgi (**Fig. 2**). This notion is supported by two lines of evidence. First, the *in vitro* addition of GGpp to isoprenoid-depleted membranes stimulated incorporation of UBIAD1 into ER-derived transport vesicles through a reaction that required ATP/GTP and cytosol as a source of COPII machinery (**Fig. 3D** and **E**). The second line of evidence indicating that GGpp modulates intracellular trafficking of UBIAD1 is provided by structural analyses of archaeal UbiA prenyltransferases, which revealed that isoprenyl substrates are positioned in the membrane-embedded active site between conserved aspartate-rich motifs (NDXXDXXXD and DXXXD) (10, 11). A residue corresponding to N102 in human UBIAD1 participates in coordination of Mg^{2+} ions that mediate interactions with the pyrophosphate group. The SCD-associated N102S mutation in UBIAD1 markedly diminishes MK-4 synthetic activity (50) and causes the mutant enzyme to become sequestered in the ER of isoprenoid-replete cells (**Fig. 4**) (12). Thus, we speculate that UBIAD1 (N102S) is retained in the ER of isoprenoid-replete cells owing to reduced affinity for membrane-embedded GGpp, which prevents its incorporation into ER-derived transport vesicles. Notably, the other 19 SCD-associated mutants of UBIAD1 are also sequestered in ER membranes (**Fig. 4**) and block reductase ERAD (**Fig. 5**). It will be important to determine whether these mutants remain in ER because of their reduced affinity for either GGpp or a component of the COPII machinery that mediates ER to Golgi transport.

A novel feature of the model shown in **Fig. 9B** is retrograde transport of UBIAD1 from the Golgi to the ER. This transport was revealed through treatment of isoprenoid-replete cells with the reductase inhibitor compactin, which caused Golgi-localized UBIAD1 to relocalize to the ER within 2 h (**Fig. 6**). A plausible mechanism for statin-induced Golgi-to-ER transport of UBIAD1 involves its sensing a decline in GGpp levels within Golgi membranes. As a result, UBIAD1 becomes incorporated into transport vesicles that carry the prenyltransferase back to the ER. However, evidence in support of an alternative scenario is provided by **Fig. 9A**, which shows that inhibition of ER export through microinjection of isoprenoid-replete cells with $Sar1^{DN}$ caused UBIAD1 to accumulate in the organelle. Together, these results support a mechanism whereby UBIAD1 constitutively cycles between the ER and Golgi, becoming trapped in ER upon sensing a drop in GGpp within ER membranes (**Fig. 9B**).

Activation of ER membrane-bound sterol regulatory element-binding proteins (SREBPs), which modulate expression of gene encoding cholesterol biosynthetic enzymes, requires transport from ER to Golgi where they encounter proteases that release transcriptionally active fragments from membranes (51, 52). This activation requires the escort protein Scap, which mediates incorporation of SREBPs into ER-derived transport vesicles bound for the Golgi (27). Cholesterol binds to Scap, causing it to bind to Insigs, which blocks incorporation of Scap and its associated SREBP into transport vesicles (53, 54). In the absence of ER export, SREBPs are no longer proteolytically activated and expression of its target genes declines. Thus, our current experiments describing the geranylgeranyl-mediated regulation of UBIAD1 trafficking represent the second example in which products of the cholesterol biosynthetic pathway control vesicular trafficking from the ER. This metabolic control of ER export is distinct from the quality control system that mediates retention of newly synthesized proteins in the ER until they are properly folded, assembled into oligomeric complexes, or have acquired posttranslational modifications (55). It is important to note that reductase does not directly contribute to intracellular trafficking of UBIAD1 (**Fig. 7**). Considering this, together with previous studies showing that sterol-induced binding of UBIAD1 to Insigs is mediated by reductase (12), we conclude that geranylgeranyl-regulated transport of UBIAD1 between the ER and the Golgi does not require the action of Insigs.

In summary, the current results indicate that UBIAD1 is a novel sensor of GGpp in ER membranes. Disruption of this sensing mechanism appears to occur in SCD and leads to the sequestration of UBIAD1 in the ER where it binds to and inhibits ERAD of reductase (**Fig.s 4** and **5**). This inhibition likely contributes to the overaccumulation of cholesterol that characterizes SCD (4, 5). Studies are now underway to expand on these observations by examining relationships between subcellular localization and enzymatic activity of UBIAD1, which will allow us to determine whether SCD-associated UBIAD1 mutants are deficient in binding to GGpp, components of the COPII machinery, or a putative escort protein. Finally, relocalization of UBIAD1 from the Golgi to the ER within 2 h of statin treatment (**Fig. 6**) indicates rapid turnover of regulatory pools of GGpp that govern intracellular transport of the prenyltransferase. Activities for kinases that phosphorylate isoprenols (such as GGOH) and phosphatases that dephosphorylate isoprenyl pyrophosphates (such as GGpp) have been described (56, 57). An exciting avenue for future investigation is to determine whether these enzymes mediate turnover of GGpp pools and contribute to intracellular transport of UBIAD1, regulation of reductase ERAD, and prenylation of proteins.

Acknowledgements

We thank Lisa Beatty, Muleya Kapaale, Hue Dao, Loren Valsin, and Ijeoma Dukes for help with tissue culture. We also thank Kristina Garland-Brasher and Gennipher Young for excellent technical assistance. This work is supported by grants from the National Institutes of Health (HL20948 and GM090216 to R.A.D.-B.; GM096070 to J.S.).

References

1. Heide, L. 2009. Prenyl transfer to aromatic substrates: genetics and enzymology. *Curr Opin Chem Biol* **13**: 171-179.

2. Nakagawa, K., Y. Hirota, N. Sawada, N. Yuge, M. Watanabe, Y. Uchino, N. Okuda, Y. Shimomura, Y. Suhara, and T. Okano. 2010. Identification of UBIAD1 as a novel human menaquinone-4 biosynthetic enzyme. *Nature* **468**: 117-121.

3. Hirota, Y., N. Tsugawa, K. Nakagawa, Y. Suhara, K. Tanaka, Y. Uchino, A. Takeuchi, N. Sawada, M. Kamao, A. Wada, T. Okitsu, and T. Okano. 2013. Menadione (vitamin K3) is a catabolic product of oral phylloquinone (vitamin K1) in the intestine and a circulating precursor of tissue menaquinone-4 (vitamin K2) in rats. *J Biol Chem* **288**: 33071-33080.

4. Orr, A., M. P. Dube, J. Marcadier, H. Jiang, A. Federico, S. George, C. Seamone, D. Andrews, P. Dubord, S. Holland, S. Provost, V. Mongrain, S. Evans, B. Higgins, S. Bowman, D. Guernsey, and M. Samuels. 2007. Mutations in the UBIAD1 gene, encoding a potential prenyltransferase, are causal for Schnyder crystalline corneal dystrophy. *PLoS One* **2**: e685.

5. Weiss, J. S., H. S. Kruth, H. Kuivaniemi, G. Tromp, P. S. White, R. S. Winters, W. Lisch, W. Henn, E. Denninger, M. Krause, P. Wasson, N. Ebenezer, S. Mahurkar, and M. L. Nickerson. 2007. Mutations in the UBIAD1 gene on chromosome short arm 1, region 36, cause Schnyder crystalline corneal dystrophy. *Invest Ophthalmol Vis Sci* **48**: 5007-5012.

6. Brownstein, S., W. B. Jackson, and R. M. Onerheim. 1991. Schnyder's crystalline corneal dystrophy in association with hyperlipoproteinemia: histopathological and ultrastructural findings. *Can J Ophthalmol* **26**: 273-279.

7. Crispin, S. 2002. Ocular lipid deposition and hyperlipoproteinaemia. *Prog Retin Eye Res* **21**: 169-224.

8. Nickerson, M. L., A. D. Bosley, J. S. Weiss, B. N. Kostiha, Y. Hirota, W. Brandt, D. Esposito, S. Kinoshita, L. Wessjohann, S. G. Morham, T. Andresson, H. S. Kruth, T. Okano, and M. Dean. 2013. The UBIAD1 prenyltransferase links menaquinone-4 [corrected] synthesis to cholesterol metabolic enzymes. *Hum Mutat* **34**: 317-329.

9. Nowinska, A. K., E. Wylegala, S. Teper, A. Lyssek-Boron, P. Aragona, A. M. Roszkowska, A. Micali, A. Pisani, and D. Puzzolo. 2014. Phenotype-genotype correlation in patients with Schnyder corneal dystrophy. *Cornea* **33**: 497-503.

10. Huang, H., E. J. Levin, S. Liu, Y. Bai, S. W. Lockless, and M. Zhou. 2014. Structure of a Membrane-Embedded Prenyltransferase Homologous to UBIAD1. *PLoS Biol* **12**: e1001911.

11. Cheng, W., and W. Li. 2014. Structural insights into ubiquinone biosynthesis in membranes. *Science* **343**: 878-881.

12. Schumacher, M. M., R. Elsabrouty, J. Seemann, Y. Jo, and R. A. DeBose-Boyd. 2015. The prenyltransferase UBIAD1 is the target of geranylgeraniol in degradation of HMG CoA reductase. *eLife* **4**:05560.

13. Goldstein, J. L., and M. S. Brown. 1990. Regulation of the mevalonate pathway. *Nature* **343**: 425-430.

14. Zhang, F. L., and P. J. Casey. 1996. Protein prenylation: molecular mechanisms and functional consequences 3. *Annu Rev Biochem* **65**: 241-269.

15. Sever, N., T. Yang, M. S. Brown, J. L. Goldstein, and R. A. DeBose-Boyd. 2003. Accelerated degradation of HMG CoA reductase mediated by binding of insig-1 to its sterol-sensing domain. *Mol Cell* **11**: 25-33.

16. Sever, N., B. L. Song, D. Yabe, J. L. Goldstein, M. S. Brown, and R. A. DeBose-Boyd. 2003. Insig-dependent ubiquitination and degradation of mammalian 3-hydroxy-3-methylglutaryl-CoA reductase stimulated by sterols and geranylgeraniol. *J Biol Chem* **278**: 52479-52490.

17. Song, B. L., N. Sever, and R. A. DeBose-Boyd. 2005. Gp78, a membrane-anchored ubiquitin ligase, associates with Insig-1 and couples sterol-regulated ubiquitination to degradation of HMG CoA reductase. *Mol Cell* **19**: 829-840.

18. Jo, Y., P. C. Lee, P. V. Sguigna, and R. A. DeBose-Boyd. 2011. Sterol-induced degradation of HMG CoA reductase depends on interplay of two Insigs and two ubiquitin ligases, gp78 and Trc8. *Proc Natl Acad Sci USA* **108**: 20503-20508.

19. Liu, T. F., J. J. Tang, P. S. Li, Y. Shen, J. G. Li, H. H. Miao, B. L. Li, and B. L. Song. 2012. Ablation of gp78 in liver improves hyperlipidemia and insulin resistance by inhibiting SREBP to decrease lipid biosynthesis. *Cell Metab* **16**: 213-225.

20. Elsabrouty, R., Y. Jo, T. T. Dinh, and R. A. DeBose-Boyd. 2013. Sterol-induced dislocation of 3-hydroxy-3-methylglutaryl coenzyme A reductase from membranes of permeabilized cells. *Mol Biol Cell* **24**: 3300-3308.

21. Morris, L. L., I. Z. Hartman, D. J. Jun, J. Seemann, and R. A. DeBose-Boyd. 2014. Sequential Actions of the AAA-ATPase Valosin-containing Protein (VCP)/p97 and the Proteasome 19 S Regulatory Particle in Sterol-accelerated, Endoplasmic Reticulum (ER)-associated Degradation of 3-Hydroxy-3-methylglutaryl-coenzyme A Reductase. *J Biol Chem* **289**: 19053-19066.

22. Rowe, T., and W. E. Balch. 1995. Expression and purification of mammalian Sarl. *Methods Enzymol* **257**: 49-53.

23. Goldstein, J. L., S. K. Basu, and M. S. Brown. 1983. Receptor-mediated endocytosis of low-density lipoprotein in cultured cells. *Methods Enzymol.* **98**: 241-260.

24. Yamamoto, T., C. G. Davis, M. S. Brown, W. J. Schneider, M. L. Casey, J. L. Goldstein, and D. W. Russell. 1984. The human LDL receptor: a cysteine-rich protein with multiple Alu sequences in its mRNA. *Cell* **39**: 27-38.

25. Mosley, S. T., M. S. Brown, R. G. Anderson, and J. L. Goldstein. 1983. Mutant clone of Chinese hamster ovary cells lacking 3-hydroxy-3 -methylglutaryl coenzyme A reductase. *J Biol Chem* **258**: 13875-13881.

26. Metherall, J. E., J. L. Goldstein, K. L. Luskey, and M. S. Brown. 1989. Loss of transcriptional repression of three sterol-regulated genes in mutant hamster cells. *J Biol Chem* **264**: 15634-15641.

27. Nohturfft, A., D. Yabe, J. L. Goldstein, M. S. Brown, and P. J. Espenshade. 2000. Regulated step in cholesterol feedback localized to budding of SCAP from ER membranes. *Cell* **102**: 315-323.

28. Diao, A., D. Rahman, D. J. Pappin, J. Lucocq, and M. Lowe. 2003. The coiled-coil membrane protein golgin-84 is a novel rab effector required for Golgi ribbon formation. *J Cell Biol* **160**: 201-212.

29. Song, B. L., and R. A. DeBose-Boyd. 2004. Ubiquitination of 3-hydroxy-3-methylglutaryl-CoA reductase in permeabilized cells mediated by cytosolic E1 and a putative membrane-bound ubiquitin ligase. *J Biol Chem* **279**: 28798-28806.

30. Rexach, M. F., and R. W. Schekman. 1991. Distinct biochemical requirements for the budding, targeting, and fusion of ER-derived transport vesicles. *J Cell Biol* **114**: 219-229.

31. Rowe, T., M. Aridor, J. M. McCaffery, H. Plutner, C. Nuoffer, and W. E. Balch. 1996. COPII vesicles derived from mammalian endoplasmic reticulum microsomes recruit COPI. *J Cell Biol.* **135**: 895-911.

32. Zhang, Y., M. Motamed, J. Seemann, M. S. Brown, and J. L. Goldstein. 2013. Point mutation in luminal loop 7 of Scap protein blocks interaction with loop 1 and abolishes movement to Golgi. *J Biol Chem* **288**: 14059-14067.

33. Nohturfft, A., R. A. DeBose-Boyd, S. Scheek, J. L. Goldstein, and M. S. Brown. 1999. Sterols regulate cycling of SREBP cleavage-activating protein (SCAP) between endoplasmic reticulum and Golgi. *Proc Natl Acad Sci USA* **96**: 11235-11240.

34. Llopis, J., J. M. McCaffery, A. Miyawaki, M. G. Farquhar, and R. Y. Tsien. 1998. Measurement of cytosolic, mitochondrial, and Golgi pH in single living cells with green fluorescent proteins. *Proc Natl Acad Sci USA* **95**: 6803-6808.

35. Banting, G., and S. Ponnambalam. 1997. TGN38 and its orthologues: roles in post-TGN vesicle formation and maintenance of TGN morphology. *Biochim Biophys Acta* **1355**: 209-217.

36. Nakamura, N., C. Rabouille, R. Watson, T. Nilsson, N. Hui, P. Slusarewicz, T. E. Kreis, and G. Warren. 1995. Characterization of a cis-Golgi matrix protein, GM130. *J Cell Biol* **131**: 1715-1726.

37. Thyberg, J., and S. Moskalewski. 1985. Microtubules and the organization of the Golgi complex. *Exp Cell Res* **159**: 1-16.

38. Shima, D. T., K. Haldar, R. Pepperkok, R. Watson, and G. Warren. 1997. Partitioning of the Golgi apparatus during mitosis in living HeLa cells. *J Cell Biol* **137**: 1211-1228.

39. Barlowe, C. K., and E. A. Miller. 2013. Secretory protein biogenesis and traffic in the early secretory pathway. *Genetics* **193**: 383-410.

40. Jensen, D., and R. Schekman. 2011. COPII-mediated vesicle formation at a glance. *J Cell Sci* **124**: 1-4.

41. Sever, N., P. C. W. Lee, B. L. Song, R. B. Rawson, and R. A. DeBose-Boyd. 2004. Isolation of Mutant Cells Lacking Insig-1 through Selection with SR-12813, an Agent That Stimulates Degradation of 3-Hydroxy-3-methylglutaryl-Coenzyme A Reductase. *J Biol Chem* **279**: 43136-43147.

42. Cole, N. B., J. Ellenberg, J. Song, D. DiEuliis, and J. Lippincott-Schwartz. 1998. Retrograde transport of Golgi-localized proteins to the ER. *J Cell Biol* **140**: 1-15.

43. Storrie, B., J. White, S. Rottger, E. H. Stelzer, T. Suganuma, and T. Nilsson. 1998. Recycling of golgi-resident glycosyltransferases through the ER reveals a novel pathway and provides an explanation for nocodazole-induced Golgi scattering. *J Cell Biol* **143**: 1505-1521.

44. Sengupta, P., P. Satpute-Krishnan, A. Y. Seo, D. T. Burnette, G. H. Patterson, and J. Lippincott-Schwartz. 2015. ER trapping reveals Golgi enzymes continually revisit the ER through a recycling pathway that controls Golgi organization. *Proc Natl Acad Sci U S A* **112**: E6752-6761.

45. Nebenfuhr, A., C. Ritzenthaler, and D. G. Robinson. 2002. Brefeldin A: deciphering an enigmatic inhibitor of secretion. *Plant Physiol* **130**: 1102-1108.

46. Lippincott-Schwartz, J., L. C. Yuan, J. S. Bonifacino, and R. D. Klausner. 1989. Rapid redistribution of Golgi proteins into the ER in cells treated with brefeldin A: evidence for membrane cycling from Golgi to ER. *Cell* **56**: 801-813.

47. D'Arcangelo, J. G., K. R. Stahmer, and E. A. Miller. 2013. Vesicle-mediated export from the ER: COPII coat function and regulation. *Biochim Biophys Acta* **1833**: 2464-2472.

48. Bartz, R., L. P. Sun, B. Bisel, J. H. Wei, and J. Seemann. 2008. Spatial separation of Golgi and ER during mitosis protects SREBP from unregulated activation. *EMBO J* **27**: 948-955.

49. Seemann, J., E. Jokitalo, M. Pypaert, and G. Warren. 2000. Matrix proteins can generate the higher order architecture of the Golgi apparatus. *Nature* **407**: 1022-1026.

50. Hirota, Y., K. Nakagawa, N. Sawada, N. Okuda, Y. Suhara, Y. Uchino, T. Kimoto, N. Funahashi, M. Kamao, N. Tsugawa, and T. Okano. 2015. Functional Characterization of the Vitamin K2 Biosynthetic Enzyme UBIAD1. *PLoS One* **10**: e0125737.

51. Goldstein, J. L., R. A. DeBose-Boyd, and M. S. Brown. 2006. Protein sensors for membrane sterols. *Cell* **124**: 35-46.

52. DeBose-Boyd, R. A., M. S. Brown, W. P. Li, A. Nohturfft, J. L. Goldstein, and P. J. Espenshade. 1999. Transport-dependent proteolysis of SREBP: relocation of site-1 protease from Golgi to ER obviates the need for SREBP transport to Golgi. *Cell* **99**: 703-712.

53. Radhakrishnan, A., L. P. Sun, H. J. Kwon, M. S. Brown, and J. L. Goldstein. 2004. Direct Binding of Cholesterol to the Purified Membrane Region of SCAP; Mechanism for a Sterol-Sensing Domain. *Mol Cell* **15**: 259-268.

54. Sun, L. P., J. Seemann, J. L. Goldstein, and M. S. Brown. 2007. From the Cover: Sterol-regulated transport of SREBPs from endoplasmic reticulum to Golgi: Insig renders sorting signal in Scap inaccessible to COPII proteins. *Proc Natl Acad Sci USA* **104**: 6519-6526.

55. Guerriero, C. J., and J. L. Brodsky. 2012. The delicate balance between secreted protein folding and endoplasmic reticulum-associated degradation in human physiology. *Phys Rev* **92**: 537-576.

56. Crick, D. C., D. A. Andres, and C. J. Waechter. 1997. Novel salvage pathway utilizing farnesol and geranylgeraniol for protein isoprenylation. *Biochem Biophys Res Commun* **237**: 483-487.

57. Miriyala, S., T. Subramanian, M. Panchatcharam, H. Ren, M. I. McDermott, M. Sunkara, T. Drennan, S. S. Smyth, H. P. Spielmann, and A. J. Morris. 2010. Functional characterization of the atypical integral membrane lipid phosphatase PDP1/PPAPDC2 identifies a pathway for interconversion of isoprenols and isoprenoid phosphates in mammalian cells. *J Biol Chem* **285**: 13918-13929.

58. Liscum, L., K. L. Luskey, D. J. Chin, Y. K. Ho, J. L. Goldstein, and M. S. Brown. 1983. Regulation of 3-hydroxy-3-methylglutaryl coenzyme A reductase and its mRNA in rat liver as studied with a monoclonal antibody and a cDNA probe. *J Biol Chem* **258**: 8450-8455.

Figure Legends

Fig. 1. Kinetics of geranylgeranyl-induced transport of UBIAD1 from the ER to the Golgi. SV-589 (A and B) and SV-589/pMyc-UBIAD1 (C) cells were set up on day 0 at 8 X 10^4 cells per well of six-well plates with glass coverslips in medium A containing 10% FCS. On day 1, cells were depleted of isoprenoids though incubation in medium A containing 10% LPDS, 10 µM sodium compactin, and 50 µM sodium mevalonate. After 16 h at 37 ºC, cells were refed medium A containing 10% LPDS, 10 µM compactin, and 30 µM geranylgeraniol (GGOH). In (B), some of the cells also received 50 µM cycloheximide. Following incubation for the indicated period of time (A and C) or 4 h (B) at 37 ºC, cells were fixed and analyzed by immunofluorescence microscopy using IgG-H8 (against endogenous UBIAD1) and IgG-9E10 (against transfected Myc-UBIAD1) using a Zeiss Axio Observer Epifluorescence microscope as described in "Materials and Methods." Scale bar is 10 microns. (D) CHO-7/pGFP-Scap cells were set up on day 0 at 6 X 10^4 cells per well of six-well plates with glass coverslips in medium B supplemented with 5% LPDS. On day 1, cells were transfected with pCMV-Myc-UBIAD1 (1 µg/dish) as described in "Materials and Methods." Four h after transfection, cells received a direct addition of medium B containing either 5% FCS (panels 1 and 2) or 5% LPDS (panels 3 and 4) (final concentrations). Following incubation for 16 h at 37 ºC, the dishes received medium B containing either 5% FCS, 1% hydroxypropyl β-cyclodextrin (HPCD), 10 µg/ml cholesterol, and 25 µg/ml 25-hydroxycholesterol (panels 1 and 2) or 5% LPDS, 1% HPCD, and 10 µM compactin (panels 3 and 4). After 6 h at 37 ºC, cells were fixed and analyzed by immunofluorescence microscopy using IgG-9E10 (against Myc-UBIAD1) as described in (A). Scale bar is 5 microns.

Fig. 2. UBIAD1 localizes to medial-trans region of the Golgi apparatus as determined by deconvolution microscopy. SV-589/pMyc-UBIAD1 cells were set up on day 0 at 1.5 X 10^5 cells per 60-mm dish with glass coverslips in medium A containing 10% FCS. On day 1, cells were transfected with pDsRed-Golgi (3 µg/dish) as described in "Materials and Methods." Four h after transfection, cells received a direct addition of medium A containing 10% FCS (final concentration). Following incubation for 16 h at 37 ºC, cells were treated for 2 h in the absence or presence of 5 µg/ml nocodazole. Cells were then fixed and analyzed by immunofluorescence deconvolution microscopy using IgG-9E10 (against transfected Myc-UBIAD1), anti-GM130, anti-TGN46, and a 100x oil objective as described in "Materials and Methods." Pearson correlation coefficients for the indicated protein and Myc-UBIAD1 are shown in graph below images.

Fig. 3. Geranylgeranyl pyrophosphate stimulates incorporation of UBIAD1 into vesicles *in vitro*. On day 0, SV-589 cells were set up at 2.5 X 10^5 cells per 100-mm dish in medium A containing 10% FCS. On day 3, cells were switched to medium A containing 10% LPDS, 10 μM compactin, and 50 μM mevalonate. Following incubation for 16 h at 37 ºC, cells were harvested for preparation of microsomes as described in "Materials and Methods." (A-C) Aliquots of pooled microsomes were incubated at the indicated temperature (A) or 37 ºC (B and C) in the absence or presence of rat liver cytosol (0-25 μl/reaction), ATP, GTP, and an ATP-regenerating system as described in "Materials and Methods." Following incubation for 20 min (A and C) or the indicated period of time (B) at 37 ºC, reactions were centrifuged to separate vesicles and membranes that were subjected to SDS-PAGE, followed by immunoblot analysis with IgG-H8 (against UBIAD1), IgG-4H4 (against Scap), and anti-ribophorin I. (D and E) Aliquots of pooled microsomes were incubated at 37 ºC with ATP, GTP, and an ATP-regenerating system in the absence or presence of cytosol (0-40 μl/reaction) prepared from reductase-deficient UT-2 cells and the indicated concentration of geranylgeranyl pyrophosphate (GGpp) or farnesyl pyrophosphate (Fpp). After 20 min at 37 ºC, membranes and vesicles were separated by centrifugation and analyzed by immunoblot with IgG-H8 (against UBIAD1).

Fig. 4. Schnyder corneal dystrophy-associated mutants of UBIAD1 are defective in trafficking from the ER to the Golgi. SV-589 cells were set up on day 0 and transfected on day 1 with 3 μg pCMV-Myc-UBIAD1 (wild type or indicated mutant) as described in the legend to **Fig. 2**. Four h after transfection, cells received a direct addition of medium A containing 10% FCS (final concentration). After 16 h at 37 ºC, cells were fixed and analyzed by immunofluorescence microscopy using IgG-9E10 (against Myc-UBIAD1) as described in the legend to **Fig. 1**.

Fig. 5. Schnyder corneal dystrophy-associated mutants of UBIAD1 confer resistance of CHO-7 cells to growth in presence of SR-12813. CHO-7 cells were set up on day 0 at 4 X 10^5 cells per 100-mm dish in medium B containing 5% FCS. On day 1, cells were transfected with 3 μg pCMV-Myc-UBIAD1 (wild type or indicated mutant) as described in the legend to **Fig. 2**. All of the plasmids contained the G418 resistance gene *neo*. On day 2, the cells were switched to medium B containing 5% FCS and 0.7 mg/ml G418 and refed every 2-3 days. On day 14, the G418-resistant cells were trypsinized, washed in medium B containing 5% LPDS, and plated in triplicate at 1 X 10^3 cells per well of a 96-well plate containing medium B supplemented with 5% LPDS and the indicated concentration of SR-12813. The cells were refed

every 2-3 days. On day 28, the wells were washed with PBS, fixed in 95% ethanol, and stained with crystal violet. The stained plates were scanned on an Epson Perfection V700 Photo Scanner (Long Beach, CA) in transmitted light mode at a resolution of 300 dots per inch. Images were analyzed using NIH Image J software to determine the average pixel value from a circular area corresponding to each well. The resulting values were subtracted from the value obtained from an empty well that received no cells to yield arbitrary units corresponding to degree of growth of each condition tested.

Fig. 6. Depletion of nonsterol isoprenoids triggers retrograde transport of UBIAD1 from the Golgi to the ER. SV-589 (A and B) and SV-589/pMyc-UBIAD1 cells (C) were set up on day 0 at 8 X 10^4 cells per well of six-well plates with glass coverslips in medium A supplemented with 10% FCS. On day 1, cells were refed identical medium; some of the cells in (C) were switched to medium A containing 10% LPDS. After 16 h at 37 ºC, cells were incubated in the identical medium for the indicated time (A), 6 h (B), or 2 h (C) in the presence of 10 µM compactin; some of the dishes in (B) also received 50 µM cycloheximide. Following treatments, cells were fixed and analyzed by immunofluorescence microscopy using IgG-H8 (against endogenous UBIAD1) and IgG-9E10 (against Myc-UBIAD1) as described in the legend to **Fig. 1**. Scale bar is 10 microns.

Fig. 7. HMG CoA reductase is not required for geranylgeranyl-mediated transport of UBIAD1 between the ER and the Golgi. CHO-K1/pMyc-UBIAD1 and UT-2/pMyc-UBIAD1 cells were set up on day 0 at 8 X 10^4 cells per well of six-well plates with glass coverslips in medium B supplemented with 5% FCS; medium for UT-2/pMyc-UBIAD1 cells was further supplemented with 200 µM mevalonate. On day 1, cells were refed medium B containing 5% FCS (no mevalonate). After 16 h at 37 ºC, cells were treated for 4 h at 37 ºC with identical medium in the absence or presence of 10 µM compactin and 30 µM geranylgeraniol (GGOH). Following treatments, cells were fixed and analyzed by immunofluorescence microscopy using IgG-9E10 (against Myc-UBIAD1) as described in the legend to **Fig. 1**. The scale bar is 5 microns.

Fig. 8. Brefeldin-A triggers relocalization of UBIAD1 from the Golgi to ER. SV-589 and SV-589/pMyc-UBIAD1 cells were set up on day 0 at 8 X 10^4 cells per well of six-well plates with glass coverslips in medium A containing 10% FCS. On day 1, cells were refed identical medium in the absence or presence of 2 µg/ml brefeldin A. Following incubation at

37 ºC for the indicated period of time (A) or 0.5 h (B), cells were fixed for immunofluorescence microscopy using IgG-H8 (against endogenous UBIAD1), IgG-9E10 (against Myc-UBIAD1), and anti-TGN46 as described in the legend to **Fig. 1**. The scale bar is 10 microns.

Fig. 9. UBIAD1 constitutively cycles between the ER and Golgi of isoprenoid-replete cells. (A) SV-589/pMyc-UBIAD1 cells on glass coverslips of six-well plates and cultured in medium A containing 10% FCS were injected with either 1 mg/ml BSA or purified $Sar1^{DN}$ protein and 2 mg/ml Texas-Red conjugated Dextran. After 3 h at 37 ºC, cells were fixed for immunofluorescence microscopy using IgG-9E10 (against UBIAD1) and anti-GM130. The results are representative of 4 independent experiments in which an average of 102 cells/experiment (408 cells total) were injected with $Sar1^{DN}$ and 132 cells/experiment (528 cell total) received BSA. Approximately 92% of cells microinjected with BSA contained Golgi-localized UBIAD1 and this was reduced to 11% upon microinjection of $Sar1^{DN}$ as depicted in the graph next to images. The scale bar is 10 microns. (B) Schematic representation of geranylgeranyl-mediated regulation of UBIAD1 transport between ER and Golgi.

FIG. 1

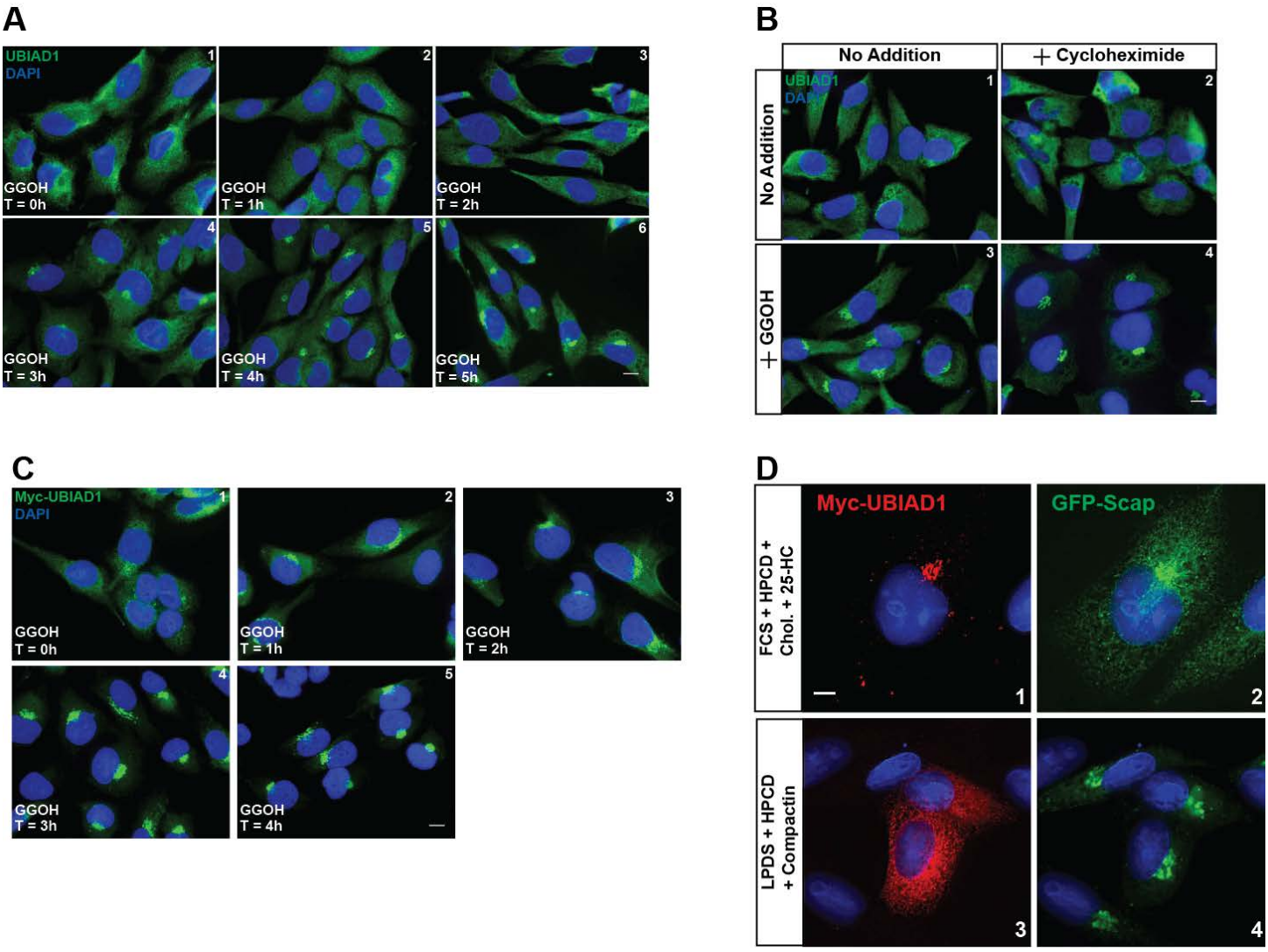

FIG. 2

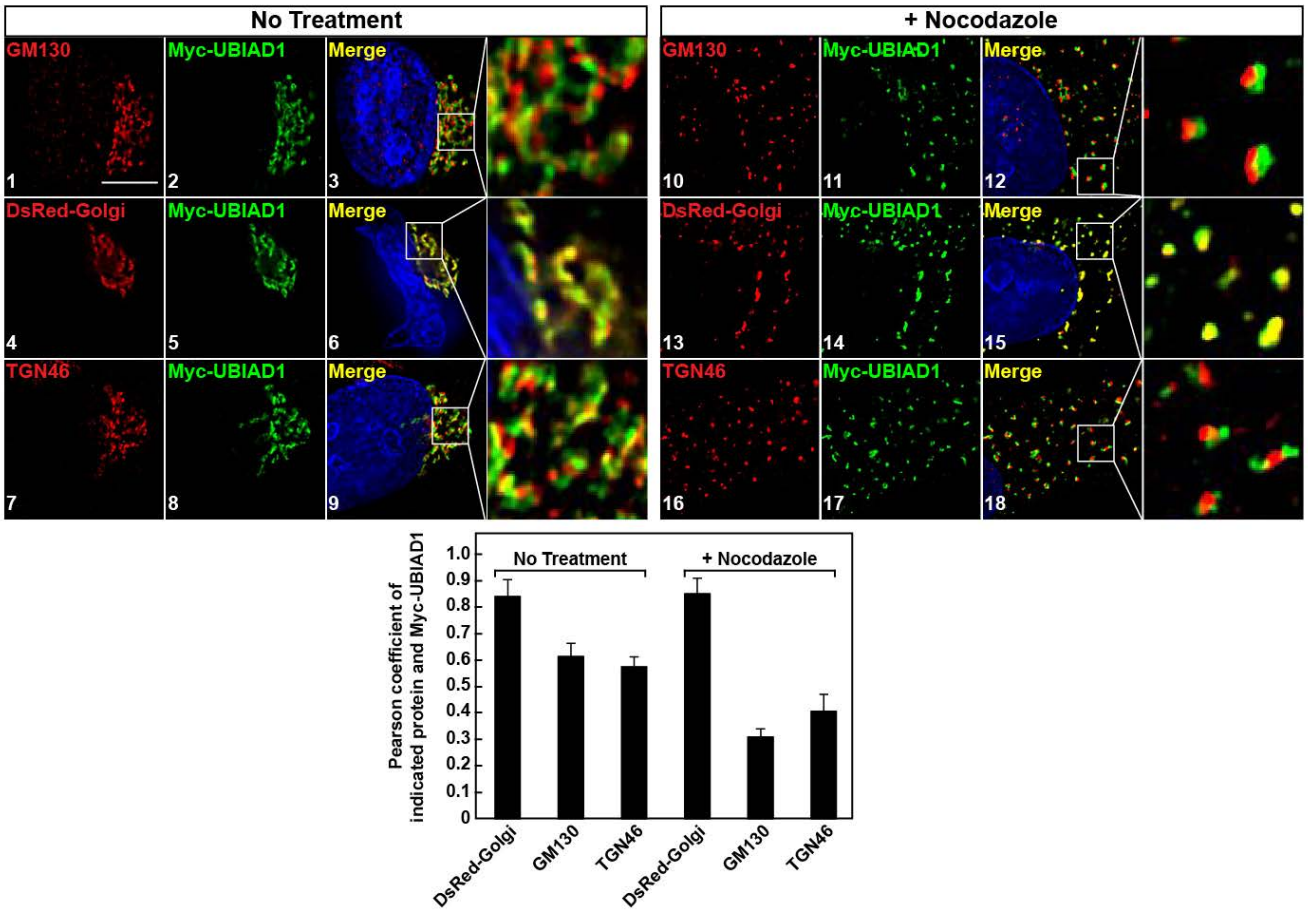

FIG. 3

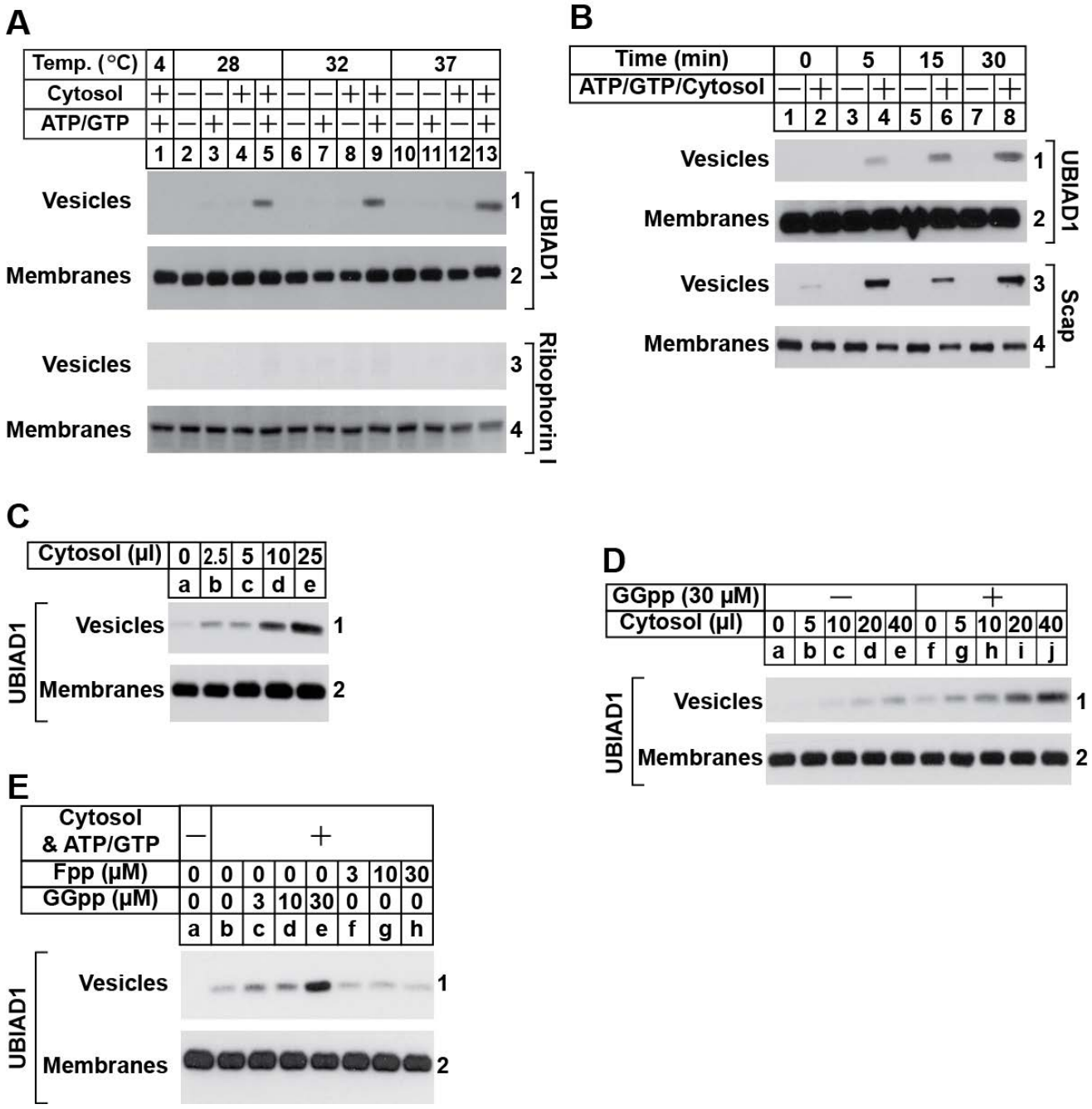

FIG. 4

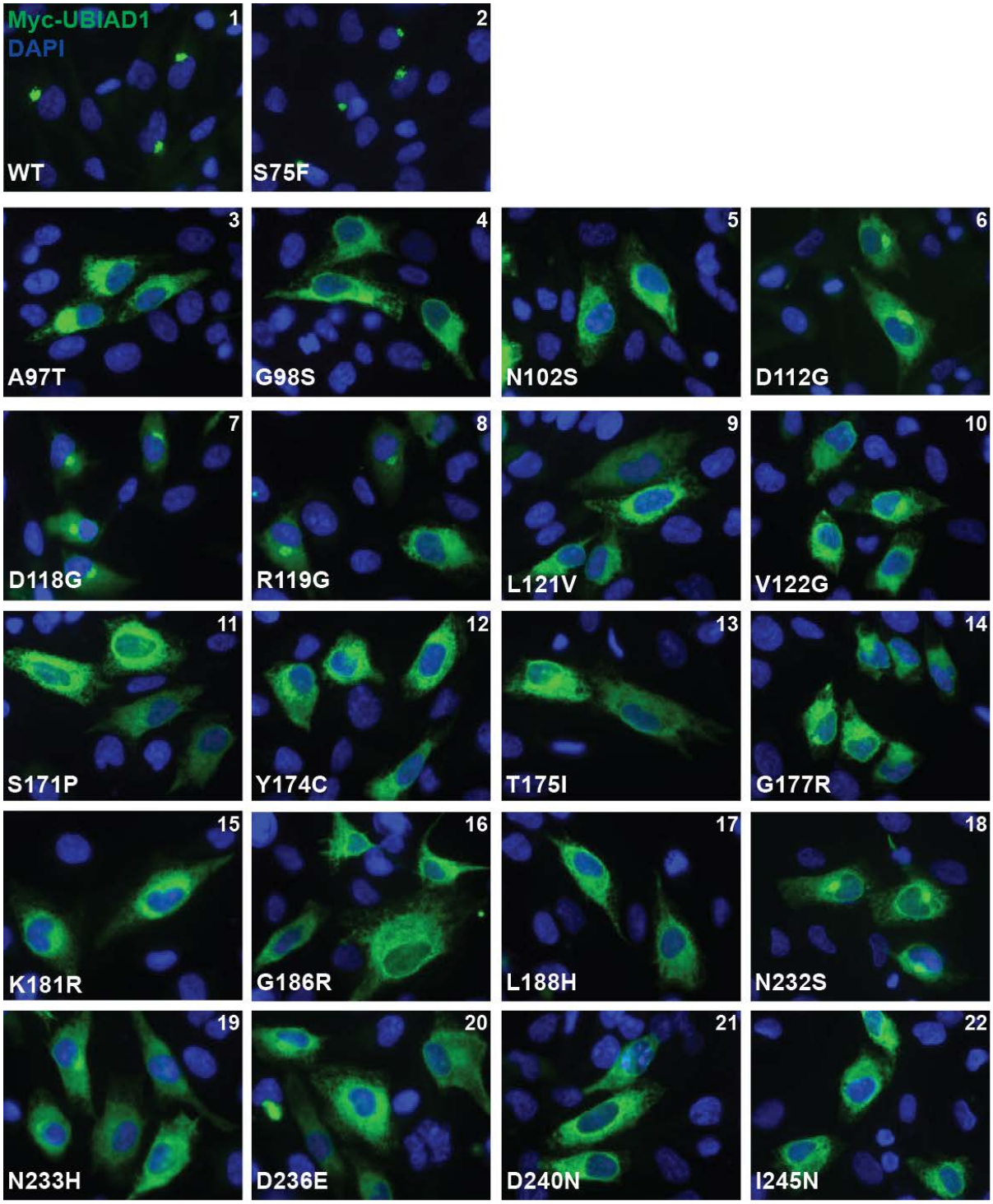

FIG. 5

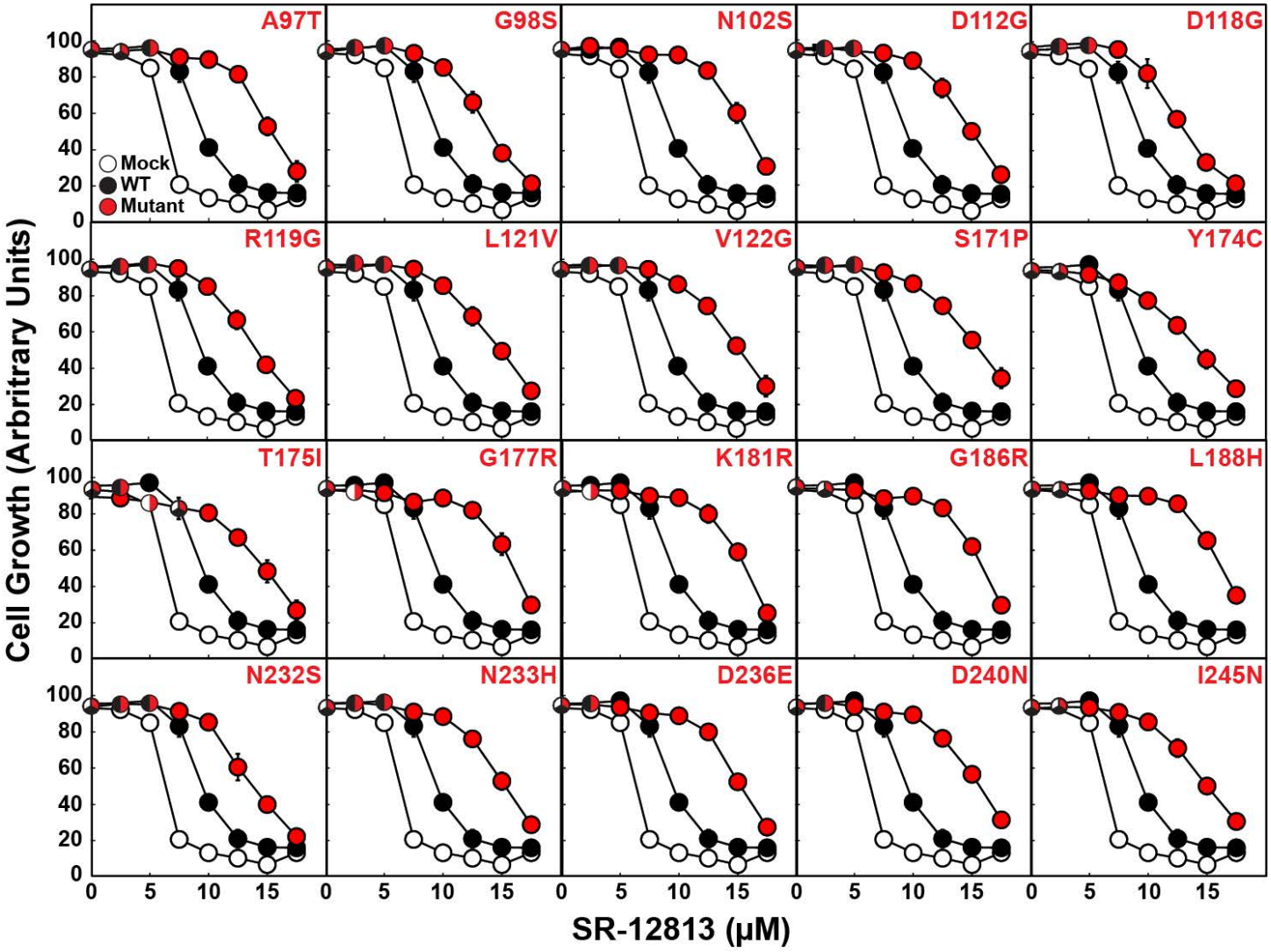

FIG. 6

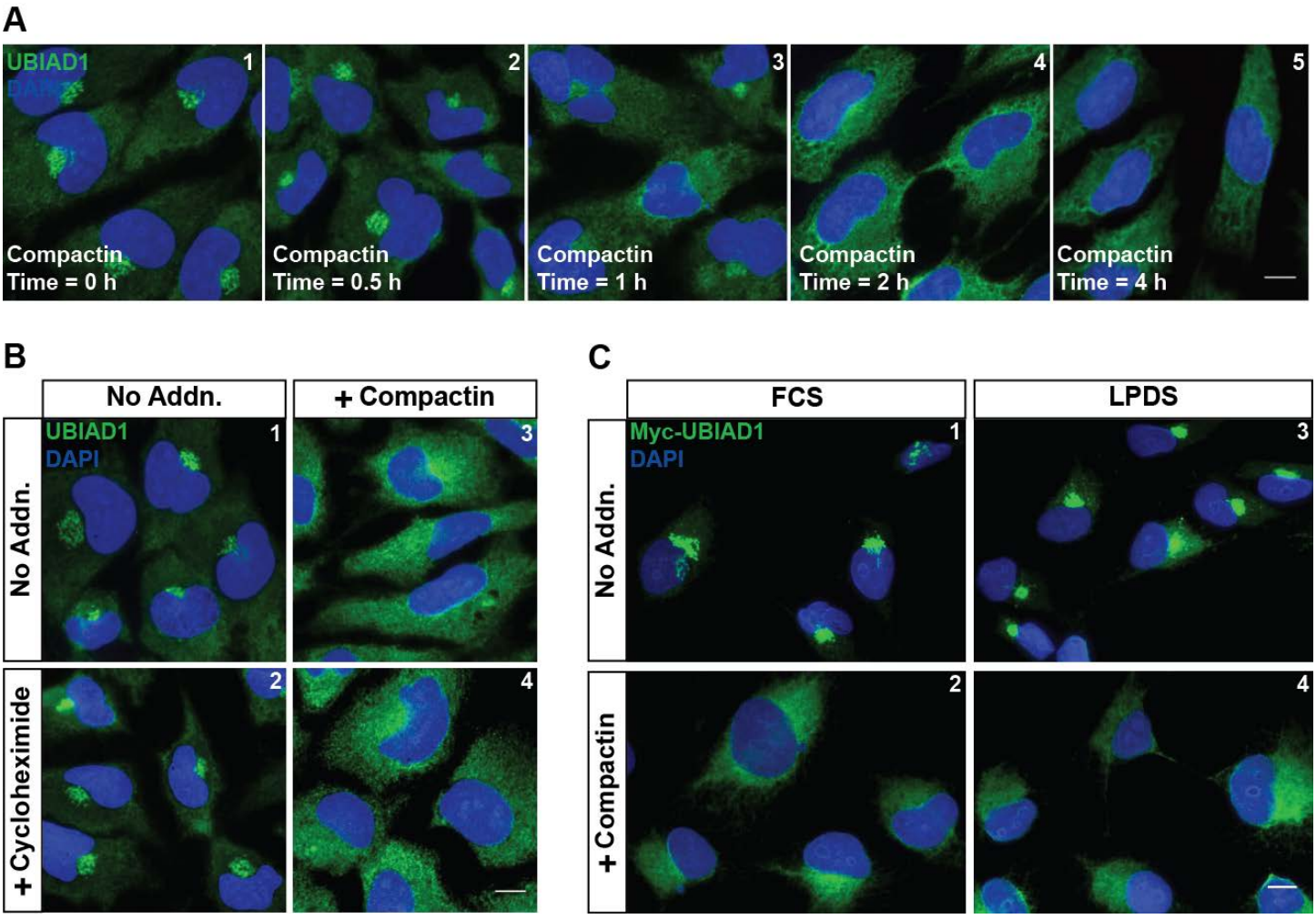

FIG. 7

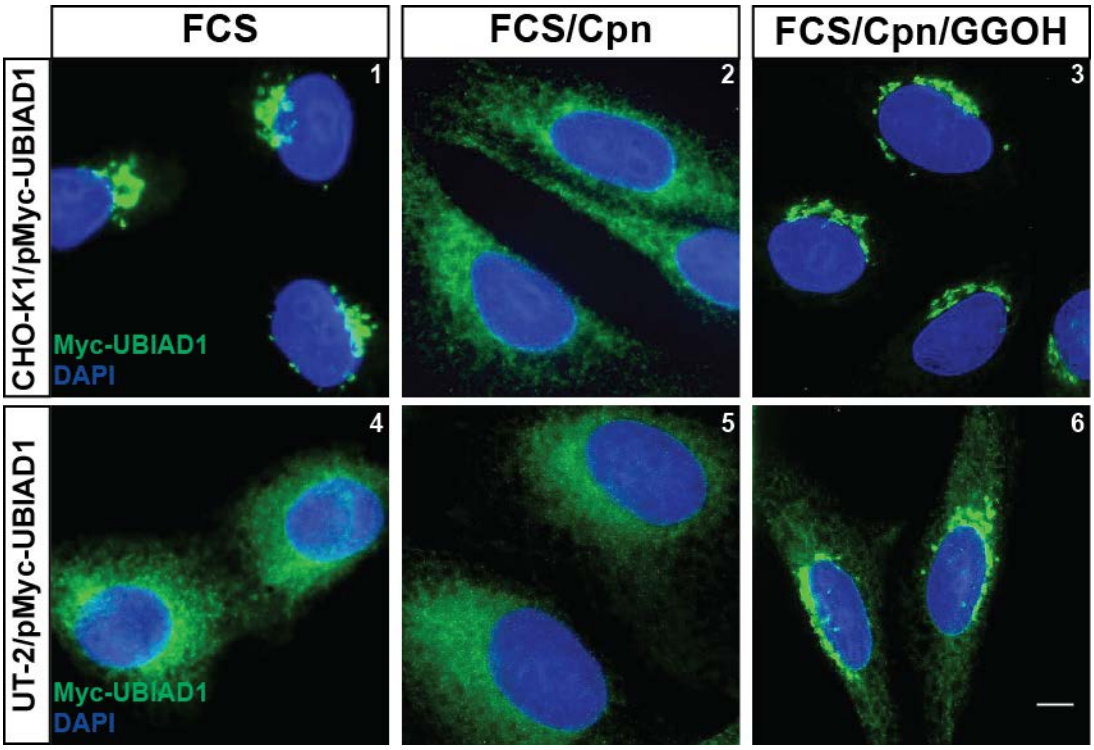

FIG. 8

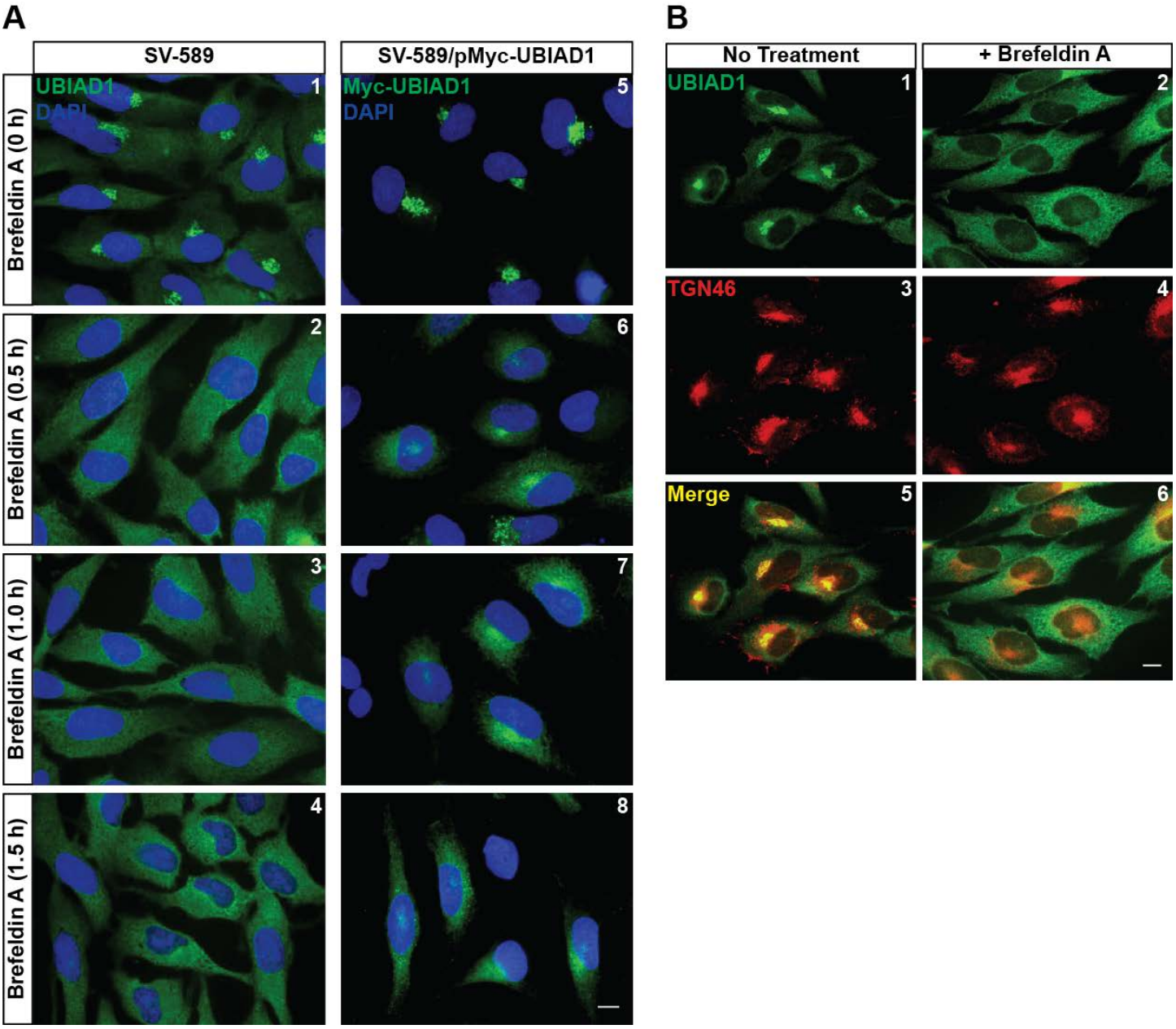

FIG. 9